Journal of Vibration Engineering & Technologies
https://doi.org/10.1007/s42417-021-00293-y

ORIGINAL PAPER

Analysis of Harmonically Forced Duffing Oscillator with Time Delay State Feedback by Incremental Harmonic Balance Method

Han Wu[1,2] · Xiaohui Zeng[1,2] · Yubiao Liu[1,2] · Jiang Lai[3]

Received: 4 November 2020 / Revised: 10 March 2021 / Accepted: 16 March 2021

Abstract

Purpose Periodic solutions of a harmonically forced Duffing oscillator with time-delay state feedback are investigated using the incremental harmonic balance method.

Method In the process of solving, the explicit effect matrix of the time delay term was derived. The stability of the periodic solutions was determined by a method which combines the continuous time approximation and multivariable Floquet theory.

Results and Conclusion On this basis, the frequency–amplitude response curve and stability characteristics of the primary resonance and the 1/3 subharmonic resonance were obtained. The stable results were compared with results obtained by the numerical method, which demonstrated the effectiveness and accuracy of the incremental harmonic balance method for the analysis of strongly nonlinear equations with time delays. The influence of the time delay and feedback control parameters on the primary and 1/3 subharmonic resonance is investigated. The periodicity of the effect of the time delay is also discussed.

Keywords Incremental harmonic balance method · Duffing oscillator · Time delay · Primary and 1/3 subharmonic resonance · Continuous time approximation

Introduction

Duffing equation is a representative differential equation in the nonlinear dynamic system, and many nonlinear vibration problems in engineering practice, such as the nonlinear behavior of the rotor, the rolling motion of the ship, and the vertical vibration of the vehicle, can be studied using this equation. For example, Naik and Singru [1] studied a quarter-car model under active control using duffing equation. Hui and Jun [2] studied an active nonlinear controller emulating a pendulum-type auto-parametric vibration absorber by Duffing oscillator. With the rapid development of active control system, the inevitable time delays in the control loops have drawn much attention. In recent years, more and more scholars pay attention to the study of Duffing system with time delay feedback control. Periodic solution of Duffing system is an important object of study, and there are two main types of study on periodic solution. One is to establish a dynamic model that is more in line with engineering practice which considers the complexity of structure, the other is to study the dynamic behavior of the system under complex excitation.

Hu et al. [3] studied the primary and 1/3 sub-harmonic resonance of a harmonically forced Duffing oscillator under state feedback control with a time delay using the method of multiple scales. Cantis´an et al. [4] analyzed the delay-induced resonance in a harmonically forced Duffing oscillator under position feedback control. Qiang et al. [5] analyzed the two-degree-of-freedom coupling Duffing system with time delay by multi-frequency homotopy analysis method. Based on the singular perturbation theory, Bellizzi et al. [6] studied a linear oscillator subject to periodic excitation coupled to a nonlinear energy sink with piecewise-quadratic damping characteristics. Oishi [7] conducted a research on the periodic solution of a time delay Duffing equation. Amer et al. [8] and Siewe et al. [9] studied the parametrically excited vibration of duffing vibrator with time delay feedback control, and the studies were both conducted by asymptotic perturbation theory. Rusinek et al. [10] investigated

✉ Xiaohui Zeng
zxh@imech.ac.cn

1 Key Laboratory for Mechanics in Fluid Solid Coupling Systems, Institute of Mechanics, Chinese Academy of Sciences, Beijing 100190, China

2 School of Engineering Science, University of Chinese Academy of Sciences, Beijing 100049, China

3 Nuclear Power Institute of China, Chengdu 610213, China

Published online: 30 March 2021

the periodic solution and its stability of time delay Duffing equation. Wang and Li [11] studied the nonlinear character of a Duffing–van der Pol oscillator subjected to forced and parametric excitation using the method of multiple scales. Mitra et al. [12] studied the limit cycle oscillations and multiple entrainment phenomena in a Duffing oscillator under time-delayed displacement feedback. Jin and Hu [13] 14 studied the primary resonance of a class of Duffing system with delay feedback under narrow-band random excitation and the feedback control of a class of double time-delay system under narrow-band random excitation. Jiang et al. [15] analyzed the dynamic response of a Helmholtz–Duffing energy harvester in the region of the primary resonance by the harmonic balance method.

It is found that studied on periodic solution and its stability of Duffing system with delayed feedback control were conducted in terms of weak-nonlinearity, and primary resonance was the main object of analysis. Moreover, singular perturbation theory is the dominating analytical method, including the multi-scale method, method of averaging, energy analysis, and singularly perturbed pseudo-oscillator analysis. In practical engineering, strong nonlinear problems and sub-harmonic resonance are often encountered. The analysis of the periodic solutions of a strongly nonlinear time delay Duffing system has rarely been reported. In addition, singular perturbation theory has good adaptability to low-dimensional and weak nonlinearity systems, but it is very difficult to deal with high-dimensional and strong nonlinearity systems. Therefore, the periodic solution and its stability of a harmonically forced strong nonlinearity Duffing oscillator with time delay state feedback is analyzed in this paper, and the incremental harmonic balance (IHB) method which can be used effectively in strong nonlinear system is adopted in our study.

The IHB method was proposed by Lau and Cheung [16] in 1981. This method combines the incremental method in numerical calculations and the harmonic balance method, and it has been widely applied on the research of high-dimensional strong nonlinearities [17–26]. Many advantages of the IHB method have been listed in the literatures mentioned above. The most important one is that it can easily deal with strongly nonlinear problems. And this method is actually a semi-numerical and semi-analytical method, so with the help of computers, it can also easily deal with high-dimensional nonlinear problems. In addition, by analyzing the stability of the periodic solution obtained by the IHB method, the unstable solution of the nonlinear system can be obtained.

In this paper, a theoretical process for applying the IHB method to solve the harmonically forced Duffing oscillator with time-delay state feedback is presented. A method that combines the continuous time approximation (CTA) and multivariable Floquet theory to determine the stability of the periodic solution is introduced. The periodic solution of the primary resonance and 1/3 subharmonic resonance, as well as its stability, are investigated. The effectiveness and accuracy of the IHB method were verified by comparing the results with those of a numerical integration method. The influence of the feedback control parameters and time delay on the nonlinear resonance is discussed.

IHB Method Applied to Nonlinear System with Time-Delay State Feedback

To introduce the IHB method to analyze the nonlinear dynamics of a delayed system, the harmonically forced Duffing oscillator with time-delay control [3] is considered:

$$\frac{\mathrm{d}^2x}{\mathrm{d}t^2} + 2\zeta\frac{\mathrm{d}x}{\mathrm{d}t} + kx + \mu x^3 = 2u\cdot x\left(t-t_d\right) + 2v\cdot\frac{\mathrm{d}x\left(t-t_d\right)}{\mathrm{d}t} + f\cos\omega t. \tag{1}$$

In Eq. (1), ζ denotes the damping ratio, μ is the nonlinear stiffness coefficient, u is the displacement feedback parameter, v is the velocity feedback parameter, t_d is the time delay in the control loop, f is the excitation amplitude, and ω is the excitation frequency. In our research, $k=1$.

Letting $\tau=\omega t$, $\tau_d=\omega t_d$, Eq. (1) can be transformed to the following:

$$\omega^2x'' + 2\zeta\omega x' + x + \mu x^3 = 2u\cdot x_d + 2v\omega\cdot x_d' + f\cos\tau, \tag{2}$$

where $x_d=x(\tau-\tau_d)$, and $x_d{}'=x'\,(\tau-\tau_d)$.

(1) The first step of the IHB method is a Newton–Raphson incrementation procedure. Let x_0, x_{0d}, f_0, and ω_0 denote a vibration state, the neighborhood state can be expressed by increments, denoted by Δ:

$$x = x_0 + \Delta x, \tag{3}$$

$$x_d = x_{0d} + \Delta x_d, \tag{4}$$

$$f = f_0 + \Delta f, \tag{5}$$

$$\omega = \omega_0 + \Delta\omega. \tag{6}$$

Substituting Eqs. (3)–(6) into Eq. (2), and neglecting all small high-order terms, the linearized incremental equation is obtained as follows:

$$\begin{aligned}&\omega_0^2\Delta x'' + 2\zeta\omega_0\Delta x' + \Delta x + 3\mu x_0^2\Delta x - 2u\Delta x_d - 2v\omega_0\cdot\Delta x_d'\\ &= \overline{R} - \left[2\omega_0x_0'' + 2\zeta x_0' - 2vx_{0d}'\right]\Delta\omega + \Delta f\cos\tau,\end{aligned} \tag{7}$$

$$\overline{R} = f_0\cos\tau - \left[\omega_0^2x_0'' + 2\zeta\omega_0x_0' + x_0 + \mu x_0^3 - 2u\cdot x_{0d} - 2v\omega_0\cdot x_{0d}'\right], \tag{8}$$

where $\bar{R}$ is a corrective value, which will equal zero when x_0, x_{0d}, f_0, and ω_0 are the exact solution.

(2) The second step of the IHB method is the Galerkin procedure, i.e., the harmonic balancing process. In the harmonic balancing process, the solution, including the increments, must be expanded as Fourier series, which are substituted into the linearized incremental equation (Eq. (7)). The coefficients of the Fourier series can be obtained by setting the coefficients of the harmonic terms on both sides to be equal.

We expand the steady state and its increment into a Fourier series,

$$\begin{aligned} x_0(\tau-\tau_d) &= a_0+\sum_{k=1}^{N_0} a_k\cos\left(k\tau-k\tau_d\right)\\ &+\sum_{k=1}^{N_0} b_k\sin\left(k\tau-k\tau_d\right)=\boldsymbol{C}\boldsymbol{\Gamma}_d\boldsymbol{A},\\ \Delta x(\tau-\tau_d) &= \Delta a_0+\sum_{k=1}^{N_0} \Delta a_k\cos\left(k\tau-k\tau_d\right)\\ &+\sum_{k=1}^{N_0} \Delta b_k\sin\left(k\tau-k\tau_d\right)=\boldsymbol{C}\boldsymbol{\Gamma}_d\Delta\boldsymbol{A}. \end{aligned} \tag{11}$$

In Eq.,

$$\boldsymbol{\Gamma}_d=\begin{bmatrix} 1 & 0 & 0 & \cdots & 0 & 0 & 0 & \cdots & 0\\ 0 & \cos\left(\tau_d\right) & 0 & \cdots & 0 & -\sin\left(\tau_d\right) & 0 & \cdots & 0\\ 0 & 0 & \cos\left(2\tau_d\right) & \cdots & 0 & 0 & -\sin\left(2\tau_d\right) & \cdots & 0\\ \vdots & \vdots & \vdots & \ddots & \vdots & \vdots & \vdots & \ddots & \vdots\\ 0 & 0 & 0 & \cdots & \cos\left(N_0\tau_d\right) & 0 & 0 & \cdots & -\sin\left(N_0\tau_d\right)\\ 0 & \sin\left(\tau_d\right) & 0 & \cdots & 0 & \cos\left(\tau_d\right) & 0 & \cdots & 0\\ 0 & 0 & \sin\left(2\tau_d\right) & \cdots & 0 & 0 & \cos\left(2\tau_d\right) & \cdots & 0\\ \vdots & \vdots & \vdots & \ddots & \vdots & \vdots & \vdots & \ddots & \vdots\\ 0 & 0 & 0 & \cdots & \sin\left(N_0\tau_d\right) & 0 & 0 & \cdots & \cos\left(N_0\tau_d\right) \end{bmatrix}.$$

$$\begin{aligned} x_0(\tau) &= a_0+\sum_{k=1}^{N_c} a_k\cos k\tau+\sum_{k=1}^{N_s} b_k\sin k\tau=\boldsymbol{C}\boldsymbol{A}\\ \Delta x(\tau) &= \Delta a_0+\sum_{k=1}^{N_c} \Delta a_k\cos k\tau+\sum_{k=1}^{N_s} \Delta b_k\sin k\tau=\boldsymbol{C}\Delta\boldsymbol{A} \end{aligned}, \tag{9}$$

where

$$\begin{aligned} \boldsymbol{C} &= \left[1,\cos\tau,\cos 2\tau,\cdots,\cos N_c\tau,sin\tau,sin2\tau,\cdots,sinN_s\tau\right],\\ \boldsymbol{A} &= \left[a_0,a_1,a_2,\cdots,a_{N_c},b_1,b_2,\cdots,b_{N_s}\right]^T,\\ \Delta\boldsymbol{A} &= \left[\Delta a_0,\Delta a_1,\Delta a_2,\cdots,\Delta a_{N_c},\Delta b_1,\Delta b_2,\cdots,\Delta b_{N_s}\right]^T. \end{aligned}$$

In this paper, the key problem of using the IHB method to carry out delayed nonlinear analysis is determining how to obtain the Fourier series expression of the delayed terms x_d and Δx_d. Based on Eq. (9), the Fourier series expression of the delayed terms x_d and Δx_d can be expressed as

$$\begin{aligned} x_0(\tau-\tau_d) &= a_0+\sum_{k=1}^{N_c} a_k\cos\left(k\tau-k\tau_d\right)+\sum_{k=1}^{N_s} b_k\sin\left(k\tau-k\tau_d\right),\\ \Delta x(\tau-\tau_d) &= \Delta a_0+\sum_{k=1}^{N_c} \Delta a_k\cos\left(k\tau-k\tau_d\right)+\sum_{k=1}^{N_s} \Delta b_k\sin\left(k\tau-k\tau_d\right). \end{aligned} \tag{10}$$

Assuming $N_c=N_s=N_0$, Eq. (11) can be obtained.

$\boldsymbol{\Gamma}_d$ is the effect matrix of the time delay on the steady-state solution and its increment. It is obvious that the matrix is periodic, and we can infer that the variation of the steady-state solution is periodic as the time delay increases.

Substituting Eqs. and into Eq., we obtain the following:

$$\begin{aligned} &\omega_0^2C''\Delta\boldsymbol{A}+2\zeta\omega_0C'\Delta\boldsymbol{A}+\boldsymbol{C}\Delta\boldsymbol{A}+3\mu x_0^2\boldsymbol{C}\Delta\boldsymbol{A}-2u\boldsymbol{C}\boldsymbol{\Gamma}_d\Delta\boldsymbol{A}\\ &-2v\omega_0C'\Gamma_d\Delta\boldsymbol{A}=\overline{R}-\left[2\omega_0C''A+2\zeta C'A-2vC'\Gamma_d\boldsymbol{A}\right]\Delta\omega+\Delta f\cos\tau, \end{aligned} \tag{12}$$

$$\begin{aligned} \overline{R} =& f_0\cos\tau-\left[\omega_0^2C''A+2\zeta\omega_0C'A+\boldsymbol{C}\boldsymbol{A}\right.\\ &\left.+\mu x_0^2\boldsymbol{C}\boldsymbol{A}-2u\boldsymbol{C}\boldsymbol{\Gamma}_d\boldsymbol{A}-2v\omega_0C'\Gamma_d\boldsymbol{A}\right]. \end{aligned} \tag{13}$$

Applying Galerkin's procedure for one time-period of 2π yields

$$\begin{aligned} &\int_0^{2\pi}\delta(\boldsymbol{C}\Delta\boldsymbol{A})^T\left[\omega_0^2C''\Delta\boldsymbol{A}+2\zeta\omega_0C'\Delta\boldsymbol{A}+\boldsymbol{C}\Delta\boldsymbol{A}+3\mu x_0^2\boldsymbol{C}\Delta\boldsymbol{A}\right.\\ &\left.-2u\boldsymbol{C}\boldsymbol{\Gamma}_d\Delta\boldsymbol{A}-2v\omega_0C'\Gamma_d\Delta\boldsymbol{A}\right]d\tau\\ &=\int_0^{2\pi}\delta(\boldsymbol{C}\Delta\boldsymbol{A})^T\left[\overline{R}-\left[2\omega_0C''A+2\zeta C'A-2vC'\Gamma_d\boldsymbol{A}\right]\Delta\omega+\Delta f\cos\tau\right]d\tau \end{aligned} \tag{14}$$

We can obtain a set of linear algebraic equations in terms of $\Delta\boldsymbol{A}$, $\Delta\omega$, and ΔF, as follows:

$$\boldsymbol{K}_{mc}\Delta\boldsymbol{A}=\boldsymbol{R}+\boldsymbol{R}_{mc}\Delta\omega+\boldsymbol{R}_f\Delta F, \tag{15}$$

where

$$\boldsymbol{K}_{mc} = \omega_0^2\boldsymbol{M} + 2\omega_0 C + K + 3\boldsymbol{K}_3 - 2\boldsymbol{K}_d - 2\omega_0\boldsymbol{C}_d, \tag{16}$$

$$\boldsymbol{R} = \boldsymbol{F} - \left[\omega_0^2\boldsymbol{M} + 2\omega_0 C + K + K_3 - 2\boldsymbol{K}_d - 2\omega_0\boldsymbol{C}_d\right]A, \tag{17}$$

$$\boldsymbol{R}_{mc} = -\left[2\omega_0\boldsymbol{M} + 2\boldsymbol{C} - 2\boldsymbol{C}_d\right]\boldsymbol{A}. \tag{18}$$

$\boldsymbol{M}$, $\boldsymbol{C}$, $\boldsymbol{K}$, $\boldsymbol{K}_3$, $\boldsymbol{K}_d$, $\boldsymbol{C}_d$, $\boldsymbol{F}$, $\boldsymbol{R}_f$, and $\Delta\boldsymbol{F}$ are given in detail as follows:

$$\begin{aligned}
&\boldsymbol{M} = \int_0^{2\pi} \boldsymbol{C}^T C''\mathrm{d}\tau, C = \int_0^{2\pi} \boldsymbol{C}^T\zeta C'\mathrm{d}\tau, K = \int_0^{2\pi} \boldsymbol{C}^T\boldsymbol{C}d\tau,\\
&\boldsymbol{K}_3 = \int_0^{2\pi} \boldsymbol{C}^T\mu x_0^2\boldsymbol{C}\mathrm{d}\tau, K_d = \int_0^{2\pi} \boldsymbol{C}^T u\boldsymbol{C}\boldsymbol{\Gamma}_d\mathrm{d}\tau, C_d = \int_0^{2\pi} \boldsymbol{C}^T\upsilon C'\Gamma_d\mathrm{d}\tau,\\
&\boldsymbol{F} = \int_0^{2\pi} \boldsymbol{C}^T f_0\cos\tau\mathrm{d}\tau, \boldsymbol{R}_f = \int_0^{2\pi} \boldsymbol{C}^T\cos\tau\mathrm{d}\tau, \Delta F = \Delta f.
\end{aligned} \tag{19}$$

In Eq. (15), the number of incremental unknowns is greater than the number of equations available due to the presence of ΔF and $\Delta\omega$. If we are primarily interested in the amplitude–frequency response curves for a certain excitation amplitude, then excitation amplitude f is a constant, Δf can be set to zero. $\Delta F = 0$ can be obtained. Therefore, Eq. (15) is reduced to.

$$\boldsymbol{K}_{mc}\Delta\boldsymbol{A} = \boldsymbol{R} + \boldsymbol{R}_{mc}\Delta\omega \tag{20}$$

Eq. (20) is a set of linear algebraic equations, the number of unknowns is one more than the number of equations. In the process of solving, we can choose one of the unknowns as the control increment, such as $\Delta\omega$ or one component of $\Delta\boldsymbol{A}$. The Newton–Raphson iterative method can be used to calculate the solution when the frequency ω or one component of the amplitude $\boldsymbol{A}$ is given. The criterion for stopping an iteration is that the corrective vector $\boldsymbol{R}$ is small enough.

It is noted that incrementing the frequency ω or incrementing one component of the amplitude $\boldsymbol{A}$ is generally successful in calculating the response curves. However, it may not converge at the sharp peaks of the response curves. To automatically track the amplitude–frequency response curve, an increment arc-length method as shown in Fig. 1 is adopted in this paper. This method can overcome this shortcoming and reduce the number of iterations.

Letting x_0, x_1, x_2, and x_3 be known points, the next point x_4 can be predicted by increasing by a prescribed arc-length Δs to extrapolate the next point. If the arc length δ is used as a parameter, then with δ_i corresponding to x_i, $\delta_0 = 0$, $\delta_1 = s_1$, $\delta_2 = \delta_1 + s_2$, $\delta_3 = \delta_2 + s_3$, and $\delta_4 = \delta_3 + \Delta s$, one has

$$x_4 = \sum_{i=0}^{3}\left(\prod_{\substack{j=0\\ j\neq i}}^{3}\frac{\delta_4 - \delta_j}{\delta_i - \delta_j}\right)x_i, \tag{21}$$

where

$$s_i = \left|x_i - x_{i-1}\right| = \sqrt{\sum_{j=1}^{N_f+1}\left[x_i(j) - x_{i-1}(j)\right]^2}, \tag{22}$$

and N_f is the number of increments, i.e., the number of total degrees of freedom in Eq. (20). Further details about the arc-length increment method can be found in Cheung et al. [27].

Stability Analysis of Periodic Solutions

The stability of the steady-state solution is usually investigated by introducing a small perturbation. We let x_0 be the obtained steady-state periodic solution and introduce an offset Δx. Substituting $x = x_0 + \Delta x$ into Eq. (2), the perturbation equation can be obtained by omitting the small items of higher order,

$$\omega^2\Delta x'' + 2\zeta\omega\Delta x' + \Delta x + 3\mu x^2\Delta x - 2u\Delta x_d - 2\upsilon\omega\cdot\Delta x_d' = 0. \tag{23}$$

This formula can also be obtained by setting $\bar{R}$, $\Delta\omega$, and Δf to zero in Eq. (7). Therefore, the stability of the periodic solution of Eq. (2) corresponds to the stability of the delayed ordinary differential equation with periodic coefficient $3\mu x^2$.

For a time-delay system with periodic coefficients, we first transform the delay differential equation into a differential equation without a time delay using the finite difference CTA method. Multivariable Floquet theory can then be used to study the stability of the differential equation without a time delay and with periodic coefficients [28]. This procedure can handle systems with multiple independent time delays or systems whose periods are not integer multiples of the time delays.

(1) The finite difference CTA method.

We let

$$\boldsymbol{q} = \left[q_1, q_2\right]^{\mathrm{T}} = \left[\Delta x', \Delta x\right]^{\mathrm{T}}. \tag{24}$$

Eq. (23) can be re-written as

$$\begin{aligned}
&\dot{\boldsymbol{q}} = \boldsymbol{f}\left(\boldsymbol{q}(\tau), \boldsymbol{q}\left(\tau - \tau_d\right), \tau\right) = \boldsymbol{G}\boldsymbol{q}(\tau) + \boldsymbol{G}_d\boldsymbol{q}\left(\tau - \tau_d\right),\\
&\boldsymbol{G} = \begin{bmatrix} -\frac{2\zeta}{\omega} & -\frac{1}{\omega^2}\left(1 + 3\mu x^2\right)\\ 1 & 0\end{bmatrix}, G_d = \begin{bmatrix}\frac{2\upsilon}{\omega} & \frac{2u}{\omega^2}\\ 0 & 0\end{bmatrix}.
\end{aligned} \tag{25}$$

The state variable of the system is expressed as $\boldsymbol{q}(\tau)$, $\boldsymbol{q}(\tau - \tau_1)$, $0 < \tau_1 \le \tau_d$. Because of the delay, the state variable is infinite. The state variables with time delay $\boldsymbol{q}(\tau - \tau_1)$, $0 < \tau_1 \le \tau_d$ can be discretized using the finite difference scheme. N is an integer, and $\Delta\tau_d = \tau_d/N$. The derivative of $\boldsymbol{q}(\tau - i\cdot\tau_d)$ is replaced with the difference:

$$\dot{\boldsymbol{q}}(\tau - i\cdot\Delta\tau_d) = \frac{1}{\Delta t_d}\left[\boldsymbol{q}(\tau-(i-1)\cdot\Delta\tau_d) - \boldsymbol{q}(\tau - i\cdot\Delta\tau_d)\right]. \tag{26}$$

A finite dimensional state variable is defined as follows:

$$\begin{aligned}\boldsymbol{p}(\tau) &= \left[\boldsymbol{q}(\tau), \boldsymbol{q}(\tau-\Delta\tau_d), \boldsymbol{q}(\tau-2\Delta\tau_d), \cdots, \boldsymbol{q}(\tau-N\Delta\tau_d)\right]^T \\ &= \left[\boldsymbol{p}_1(\tau), \boldsymbol{p}_2(\tau), \boldsymbol{p}_3(\tau), \cdots, \boldsymbol{p}_{N+1}(\tau)\right]^T.\end{aligned} \tag{27}$$

A state equation based on the extended state variable can be obtained:

$$\dot{p}(\tau) = \begin{bmatrix} f\left(\boldsymbol{q}(\tau), \boldsymbol{q}(\tau-\tau_d), \tau\right) \\ \frac{1}{\Delta\tau_d}\left[\boldsymbol{p}_1(\tau) - \boldsymbol{p}_2(\tau)\right] \\ \vdots \\ \frac{1}{\Delta\tau_d}\left[\boldsymbol{p}_N(\tau) - \boldsymbol{p}_{N+1}(\tau)\right] \end{bmatrix} = \boldsymbol{R}\cdot\boldsymbol{p}(\tau), \tag{28}$$

in which

$$\boldsymbol{R} = \begin{bmatrix} \boldsymbol{G} & 0 & \cdots & 0 & \boldsymbol{G}_d \\ \frac{1}{\Delta\tau_d}\boldsymbol{I} & -\frac{1}{\Delta\tau_d}\boldsymbol{I} & & & \\ & \ddots & & & \\ & & \ddots & & \\ & & & \frac{1}{\Delta\tau_d}\boldsymbol{I} & -\frac{1}{\Delta\tau_d}\boldsymbol{I} \end{bmatrix}. \tag{29}$$

The stability of the Eq. (23) can be determined by the stability of the new state equation given by Eq. (28). In Eq. (28), $\boldsymbol{R}$ is a periodic function with a periodic coefficient $3\mu x^2$, and we apply Floquet theory to analyze its stability.

(2) Multivariable Floquet theory.

Because x_0 is a periodic function of τ, the period is 2π. Hence, $\boldsymbol{R}$ also is a periodic function with the same period as x_0. For Eq. (28), there exists a fundamental solution $\boldsymbol{\Phi}$ that satisfies the following matrix equation:

$$\begin{aligned}&\dot{\boldsymbol{\Phi}}(\tau) = \boldsymbol{R}(\tau)\boldsymbol{\Phi}(\tau), \\ &\dot{\boldsymbol{\Phi}}(\tau+T) = \boldsymbol{R}(\tau)\boldsymbol{\Phi}(\tau+T), \\ &\boldsymbol{\Phi}(\tau+T) = \boldsymbol{C}\boldsymbol{\Phi}(\tau),\end{aligned} \tag{30}$$

where $\boldsymbol{C}$ is the transition matrix. According to the Floquet theory, the stability criteria for the system is related to the eigenvalues of the transition matrix $\boldsymbol{C}$. If all the moduli of the eigenvalues of $\boldsymbol{C}$ are less than 1, the motion is bounded, and therefore the solution is stable. Otherwise, the motion is unbounded, and the solution is unstable.

We can numerically calculate a fundamental solution of Eq. (28) using the initial condition $\boldsymbol{\Phi}(0) = \boldsymbol{I}$. Then,

$$\boldsymbol{C} = \boldsymbol{\Phi}(T). \tag{31}$$

Following Friedmann's method [29], we suppose that each period T is divided into N_k intervals, and the k-th interval is denoted by $\Delta_k = \tau_k - \tau_{k\text{-}1}$. In the k-th interval, the periodic coefficient matrix $\boldsymbol{R}(\tau)$ is replaced by a constant matrix $\boldsymbol{R}_k$,

$$\boldsymbol{R}_k = \frac{1}{\Delta_k}\int_{\tau_{k-1}}^{\tau_k} \boldsymbol{R}(\xi)\mathrm{d}\xi. \tag{32}$$

The transfer matrix is given by the following formula,

$$\boldsymbol{C} = \boldsymbol{\Phi}(T) = \prod_{i=1}^{N_k}\left[\exp\left(\Delta_i\boldsymbol{R}_i\right)\right] = \prod_{i=1}^{N_k}\left[\boldsymbol{I} + \sum_{j=1}^{N_j}\frac{\left(\Delta_i\boldsymbol{R}_i\right)^j}{j!}\right]. \tag{33}$$

Comparison and Verification

Other scholars carried out some studies on Eq. (1) by different methods. To verify the accuracy and precision of the method proposed in this paper, we compared the analysis results with those of two scholars.

Oishi[7] proposed a numerical method and obtained the amplitude-frequency response curve when $\zeta = 0.05$, $\mu = 0.25$, $u = 0.125$, $v = 0$, $k = 2.25$, $t_d = 0.1$, $f = 0.76$. We made a comparison between our method and the method of Oishi, as shown in Fig. 2. The comparison results are in good agreement.

Rusinek et al.[10] analyzed the primary resonance when $\zeta = 0.05$, $\mu = 0.25$, $u = 0.025$, $v = 0$, $k = 1$, $t_d = 4.833$, $f = 0.2$ by multiscale method and Runge–Kutta integration. Figure 3 compares the amplitude frequency curve obtained by the method in this paper with the results of Rusinek et al. Comparatively, it is found that the calculation results of our method are consistent with the results of Runge–Kutta integration, and that it has higher precision

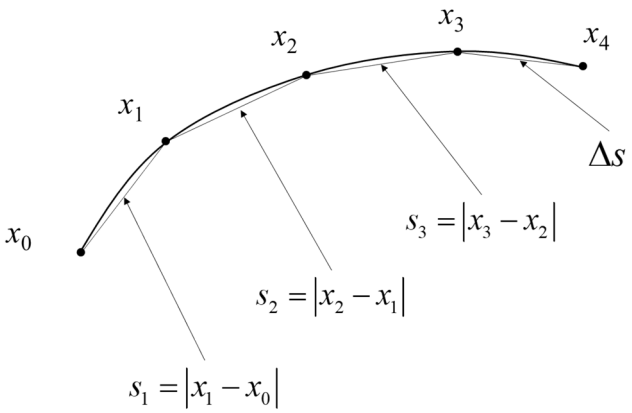

Fig. 1 Cubic extrapolation to predict the next solution point

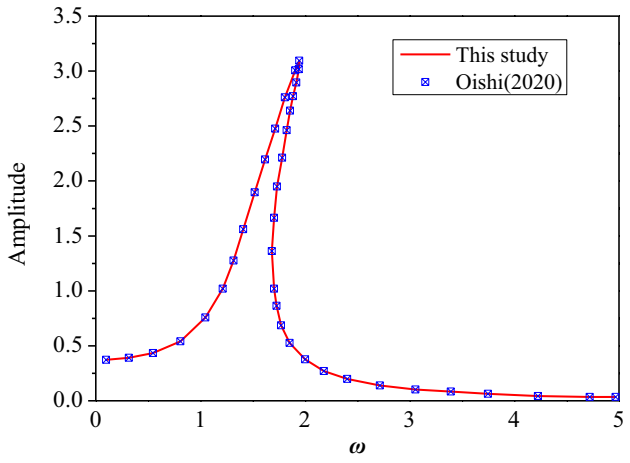

Fig. 2 Comparison with Oishi

compared with the first and the second approximations of multiscale method.

To achieve high precision, the multi-scale method needs high order approximation, which requires tedious derivation. However, the method proposed in this paper can easily achieve high order approximation analysis with the help of computer. However, compared with the multi-scale method, the method presented in this paper has some shortcomings. It can only analyze the steady-state solution or the periodic solution, but cannot obtain the transient solution.

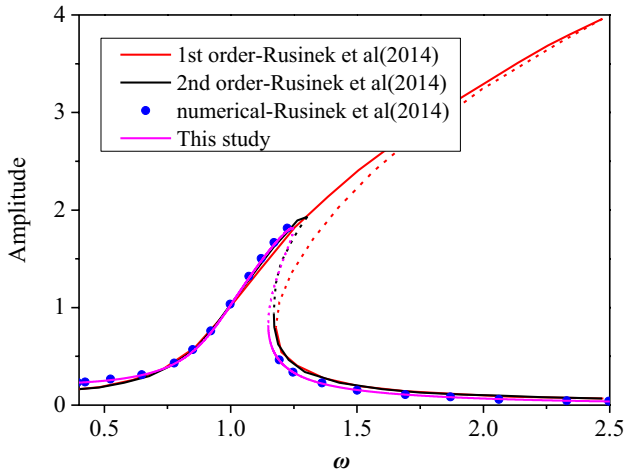

Fig. 3 Comparison with Rusienk

Primary Resonance

The amplitude–frequency curves of the primary resonance were obtained, as shown in Fig. 4. In the solution process, the number of harmonic terms was taken as $N_c = N_s = 8$, $\zeta = 0.05$, $\mu = 4.0$, $u = 0.05$, $v = -0.05$, $f = 0.5$, and $t_d = 0.0$ or 0.5. In this figure, the regions where the lines are solid are stable, i.e., the periodic solution is stable. The regions where the lines are dotted are unstable, i.e., the periodic solution is unstable. The stiffness nonlinearity μ was taken as 4.0, which indicated that the Duffing oscillator was a strongly nonlinear system with a hard spring.

Because of the positive cubic nonlinearity, the resonance peak of the amplitude–frequency curve is skewed to the right. The amplitude–frequency curve is divided into three segments. The first segment (A–C) is stable, and there are two peaks. The second segment (C–D) is unstable, and the third segment (D–E) is stable.

As the excitation frequency increases, when the second peak (point C) is reached, the periodic solution will jump

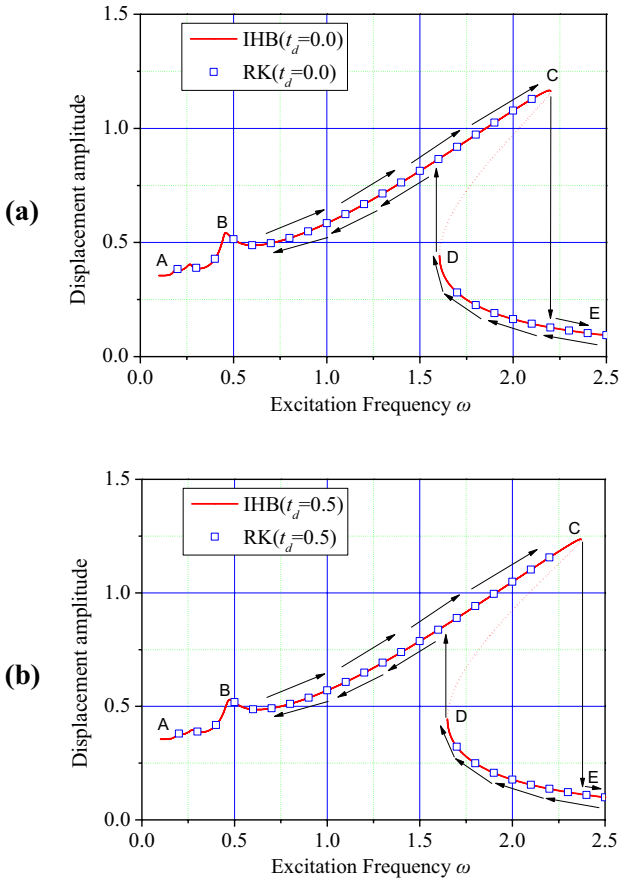

Fig. 4 Frequency–amplitude relations of the primary resonance: **a** $t_d = 0.0$; **b** $t_d = 0.5$. ($\zeta = 0.05$, $\mu = 4.0$, $u = 0.05$, $v = -0.05$, $f = 0.5$; solid line: stable, dotted line: unstable)

from the first segment to the third segment, and the amplitude will suddenly decrease. If the excitation frequency starts large (to the right of D) and decreases to point D, the periodic solution will jump from the third segment to the first segment, and the amplitude will suddenly increase. The hysteresis loops is plotted in Fig. 4 to help understand how the system jumps between branches as the excitation frequency is varied. After the time delay is taken into account, the amplitude–frequency curve is shifted further to the right, and the nonlinearity becomes more evident.

The results obtained by the fourth-order Runke–Kutta numerical integration method are plotted in Fig. 4 as square markers for comparison. The results obtained by the improved IHB method were in excellent agreement with those from Runge–Kutta method. The comparison proves that the improved IHB method is an efficient and accurate method for nonlinear systems with time delay state feedback. In addition, one of the advantages of the IHB method over the numerical integration method is that is can efficiently determine the unstable periodic solutions of nonlinear systems with time delays.

Figures 5 and 6 show the time histories and phase diagrams of the periodic solutions in the first and third segments, respectively, for $u=0.05$, $v=-0.05$, and $\omega=1.8$. In these two figures, the time history and phase diagram are very close to simple harmonic motion, because the first-order harmonic response of the periodic solutions (i.e., the main harmonic whose frequency is equal to the excitation frequency) plays a dominate role in the primary resonance.

The frequency–amplitude curves for different feedback control parameters are shown in Fig. 7. The results in the figure show that the amplitude of the periodic solution decreases with the increase in the feedback parameter, indicating that the amplitude of the periodic solution can be effectively suppressed by the increase in the feedback control parameter. In addition, compared to a case with large feedback parameters, the amplitude–frequency curve deviates more significantly to the high-frequency side when

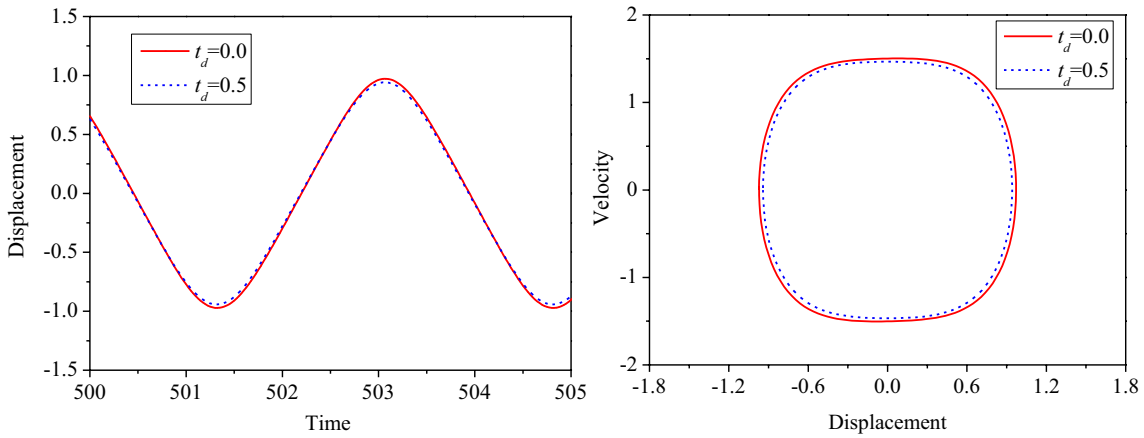

Fig. 5 Time histories and phase diagrams ($\zeta=0.05$, $\mu=4.0$, $u=0.05$, $v=-0.05$, and $\omega=1.8$ on the first segment)

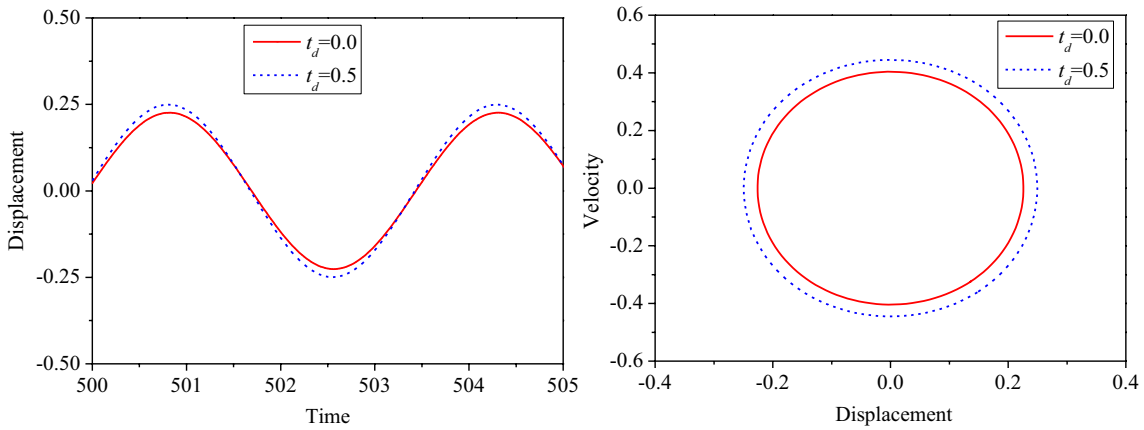

Fig. 6 Time histories and phase diagrams ($\zeta=0.05$, $\mu=4.0$, $u=0.05$, $v=-0.05$, and $\omega=1.8$ on the third segment)

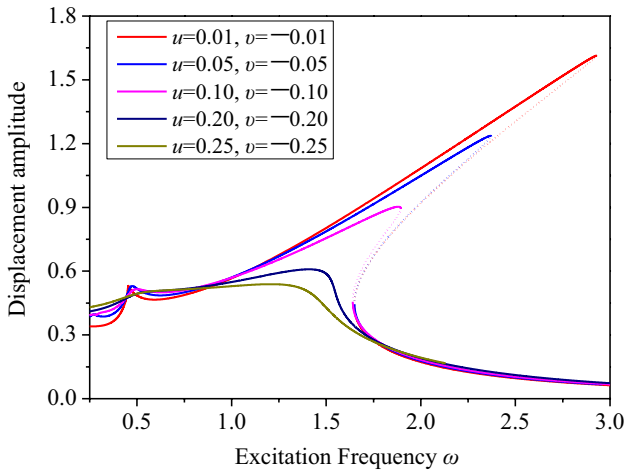

Fig. 7 Frequency–amplitude relations of the primary resonance for different feedback control parameters (t_d=0.5; solid line: stable, dotted line: unstable)

the feedback parameters are small, indicating that when the feedback parameters are small, the nonlinearity is more evident. When the feedback parameter is large enough, the unstable segment of the amplitude–frequency curve will become stable, and the periodic solution will not jump with the increase or decrease of the excitation frequency. It is clear that there is a critical parameter choice for which hysteresis disappears and the solution becomes monotonic.

1/3 Subharmonic Resonance

To study the 1/3 subharmonic resonance of the controlled system, Eq. is rewritten as.

$$\omega^2 x'' + 2\zeta\omega x' + x + \mu x^3 = 2u \cdot x_d + 2v\omega \cdot x'_d + f\cos 3\tau. \tag{34}$$

The improved IHB method was applied to analyze this formula. In this section, we set $\zeta = 0.05$, $\mu = 0.05$ or 0.5, $u = 0.05$, $v = -0.05$, $f = 40$, and $t_d = 0$ or 0.5. The frequency–amplitude curves of the 1/3 subharmonic resonance when μ is taken as 0.05 and 0.5 are shown in Figs. 8 and 9, respectively. The solid line segments are stable, and the dotted line segments are unstable. The results of the two figures show that the larger the excitation frequency, the larger the vibration amplitude. The amplitude–frequency curve of the 1/3 subharmonic resonance has the shape of a Fig. 8. The stable and unstable segments intersect each other, and the amplitudes of the stable and unstable periodic solutions change on either side of the intersection point.

In Fig. 8, μ is taken as 0.05. When $t_d = 0.5$, the amplitude–frequency response curve is basically consistent with that for $t_d = 0.0$, but the excitation frequency range where

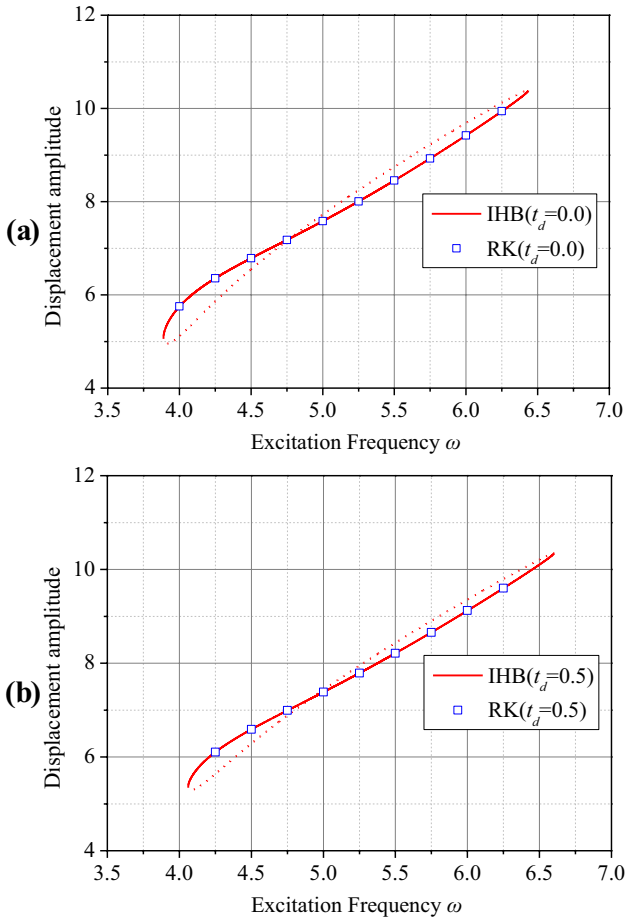

Fig. 8 Frequency–amplitude relations of the 1/3 subharmonic resonance: **a** t_d=0; **b** t_d=0.5. (ζ=0.05, μ=0.05, u=0.05, v=−0.05, f=40; solid line: stable, dotted line: unstable)

the 1/3 subharmonic resonance occurs is shifted in the positive direction. However, the case when μ was taken as 0.5 is shown in Fig. 9. In addition to this shift when $t_d = 0.5$, the excitation frequency range where the 1/3 subharmonic resonance occurs is much larger than the range when $t_d = 0.0$. This shows that the time delay has a great influence on the frequency range of the 1/3 subharmonic resonance.

In addition, the improved IHB method is also compared with the fourth-order Runge–Kutta method. The results of the two methods were in good agreement, which further verified the correctness of the method.

Based on Eq., the harmonic amplitude of the periodic solution for each order can be calculated by.

$$A_i = \sqrt{a_k^2 + b_k^2}. \tag{35}$$

The curves relating the amplitudes of the first and third harmonics and the excitation frequency corresponding to the results in Figs. 8 and 9 are given Figs. 10 and 11, respectively. The results show that there is a subharmonic vibration

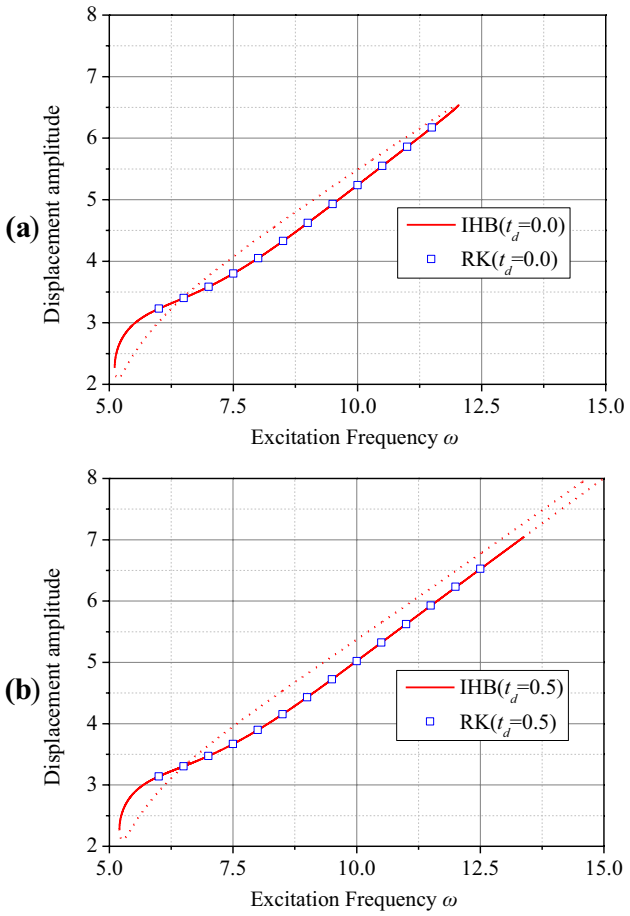

Fig. 9 Frequency–amplitude relations of the 1/3 subharmonic resonance: **a** $t_d=0$; **b** $t_d=0.5$. ($\zeta=0.05$, $\mu=0.5$, $u=0.05$, $v=-0.05$, $f=40$; solid line: stable, dotted line: unstable)

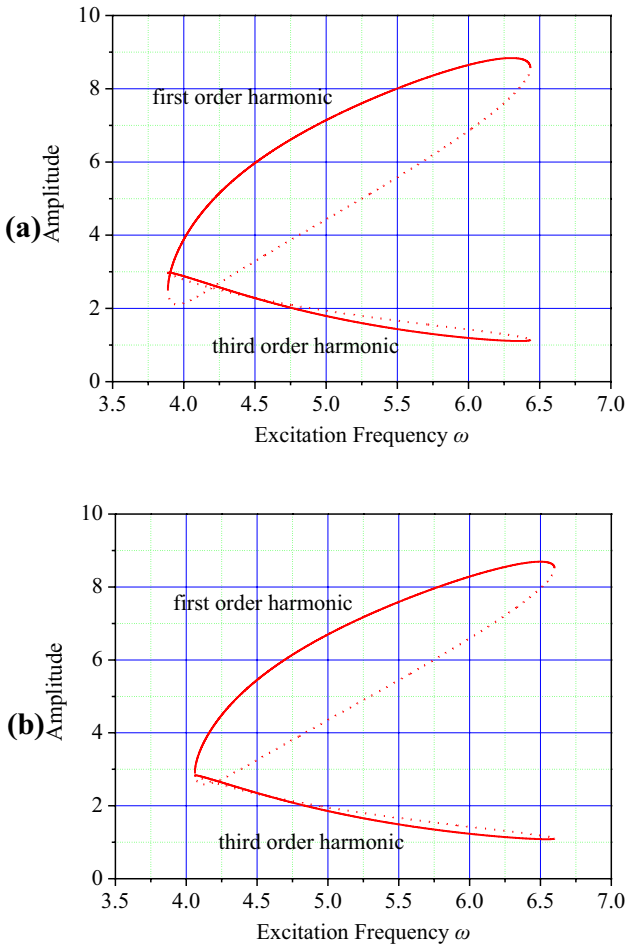

Fig. 10 First-order and third-order harmonic frequency–amplitude relations of the 1/3 subharmonic resonance: **a** $t_d=0$; (b) $t_d=0.5$. ($\zeta=0.05$, $\mu=0.05$, $u=0.05$, $v=-0.05$, $f=40$; solid line: stable, dotted line: unstable)

(i.e., the first order harmonic) whose frequency is 1/3 the excitation frequency. This indicates that, due to the cubic nonlinearity, the Duffing oscillator exhibits 1/3 subharmonic resonance.

In Figs. 10 and 11, the amplitude–frequency curves of the first-order harmonic show that the larger the frequency is, the larger the amplitude is. On the contrary, the amplitude of the third-order harmonic decreases as the excitation frequency increases. Under the same excitation frequency in the first-order harmonic, the amplitude of the stable solution is larger than that of the unstable solution. However, there is an intersection between the stable segment of the first-order harmonic and the unstable segment of the third-order harmonic, the relative sizes of the stable and unstable solutions on either sides of the intersection are opposite.

As shown in Figs. 8 and 9, the amplitude–frequency curve of the 1/3 subharmonic resonance has a Fig. 8 shape, and the stable and unstable segments intersect each other. Based on Figs. 10 and 11, this is caused by the third-order harmonic vibration.

Figures 12 and 13 show the time history curves and phase diagrams of the stable periodic solution in Fig. 7 when the excitation frequency is 4.5 and 6.0, respectively. Figures 14 and 15 show the time history curves and phase diagrams of the stable periodic solution in Fig. 9 when the excitation frequency is 7.5 and 10.0, respectively.

Comparing Figs. 12 and 13 as well as Figs. 14 and 15, it is evident that the time-history curves and phase diagrams are closer to a simple harmonic vibration if the frequency is larger. This can be explained by Figs. 10 and 11. With the increase in the excitation frequency, the amplitude of the first-order harmonic (i.e., the vibration whose frequency is 1/3 the excitation frequency) becomes larger

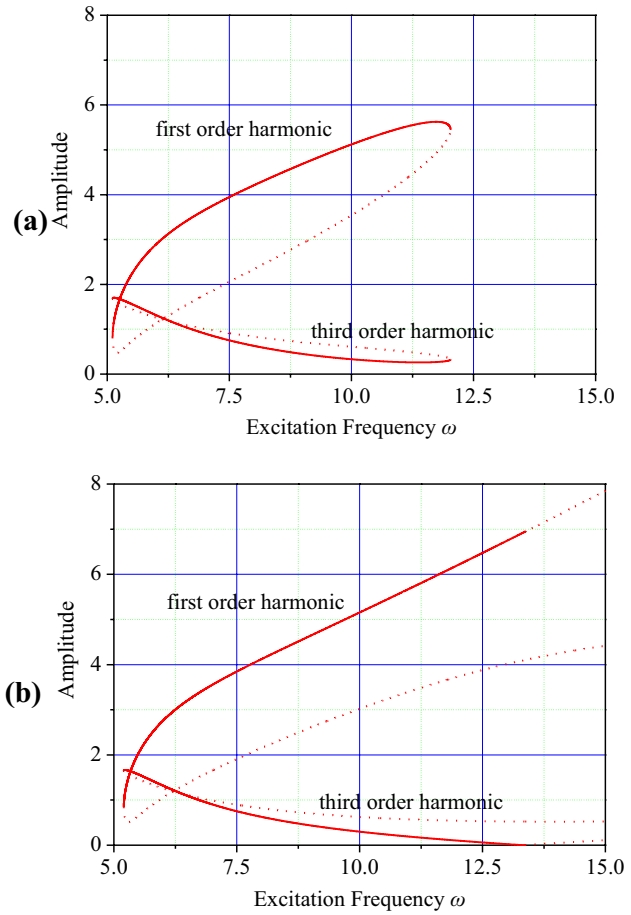

Fig.11 First-order and third-order harmonic frequency–amplitude relations of the 1/3 subharmonic resonance: **a** $t_d=0$; **b** $t_d=0.5$. ($\zeta=0.05$, $\mu=0.5$, $u=0.05$, $v=-0.05$, $f=40$; solid line: stable, dotted line: unstable)

and larger, while the amplitude of the third-order harmonic become smaller. Therefore, when the excitation frequency is larger, the first-order harmonic will become dominant in the periodic solution, and the time-history curve and phase diagram become closer to the single-frequency simple harmonic vibration.

Periodicity of the Effect of Time Delay

As shown by Eq. (11), the effect matrix of the time delay $\boldsymbol{\Gamma}_d$ is a periodic function of t_d, and its period is $2\pi/\omega$. Thus, we infer that effect of the time delay on the nonlinear response is periodic. The relationship between the periodic solution amplitude and the time delay with different excitation frequencies ω was calculated and is shown in Fig. 16. The amplitude of the periodic solution varies periodically with the time delay, and the period is $2\pi/\omega$.

Xu [30] investigated the periodic solutions of nonlinear systems with delays by applying averaging methods, and the periodicity of the effect of the delay on the periodic solution and its stability were proven in their studies. Based on the analysis of the IHB method, the same conclusion was obtained. This mechanism for this effect was further confirmed in this analysis.

Conclusion

In this paper, the explicit effect matrix of the time delay is obtained by deriving the harmonic expansion formula. A method that combines the CTA and Floquet theory to analyze the stability of the periodic solution is introduced. On this basis, the primary and 1/3 subharmonic resonance of a harmonically strongly nonlinear Duffing oscillator with time-delay state feedback is presented. The stability results are compared with the results obtained by the Runge–Kutta integration technique. The results obtained by both methods were in good agreement. The results demonstrated that the

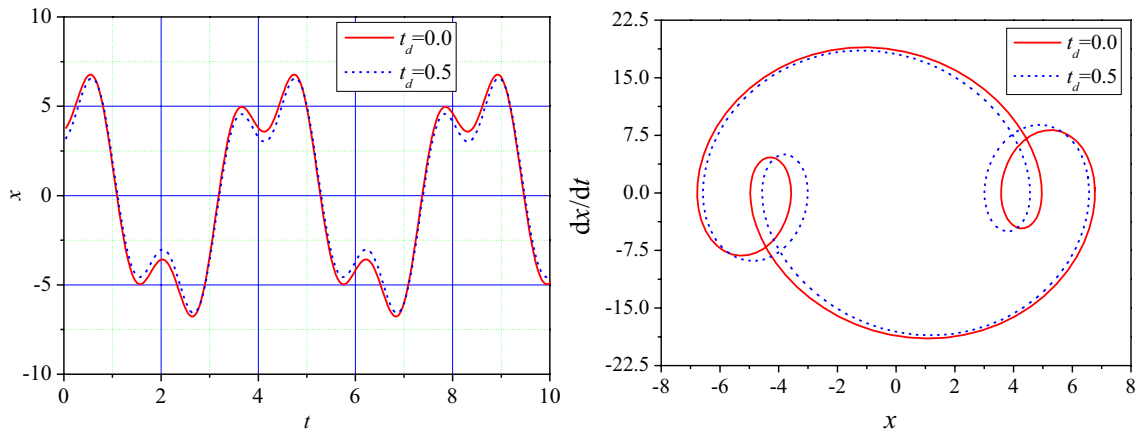

Fig. 12 Time histories and phase diagrams (stable solutions when $\zeta=0.05$, $\mu=0.05$, $u=0.05$, $v=-0.05$, $\omega=4.5$, $t_d=0$ and 0.5)

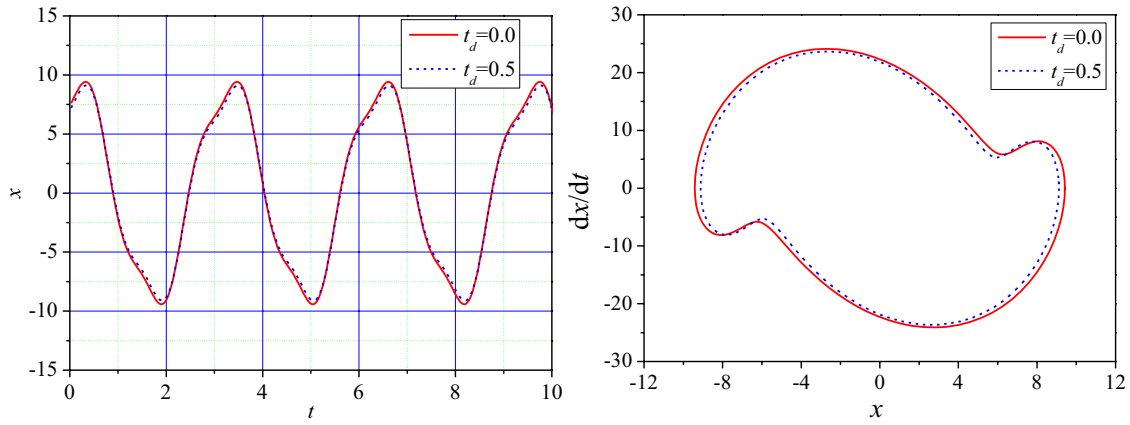

Fig. 13 Time histories and phase diagrams (stable solutions when $\zeta = 0.05$, $\mu = 0.05$, $u = 0.05$, $v = -0.05$, $\omega = 6.0$, $t_d = 0$ and 0.5)

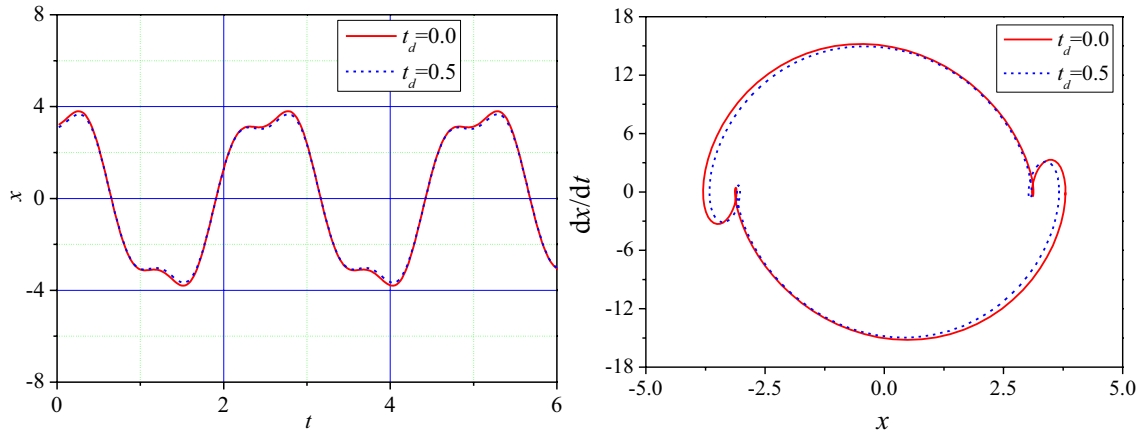

Fig. 14 Time histories and phase diagrams (stable solutions when $\zeta = 0.05$, $\mu = 0.5$, $u = 0.05$, $v = -0.05$, $\omega = 7.5$, $t_d = 0$ and 0.5)

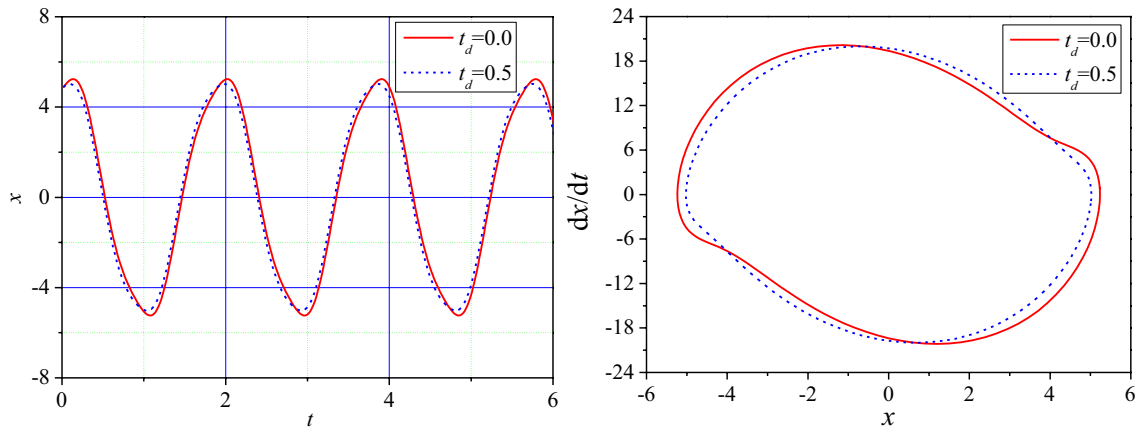

Fig. 15 Time histories and phase diagrams (stable solutions when $\zeta = 0.05$, $\mu = 0.5$, $u = 0.05$, $v = -0.05$, $\omega = 10.0$, $t_d = 0$ and 0.5)

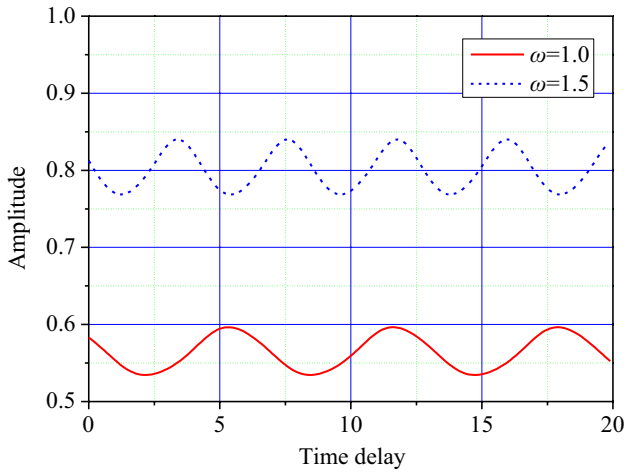

Fig. 16 Relationship between periodic solution amplitude and time delay ($\zeta=0.05$, $\mu=4.0$, $u=0.05$, $v=-0.05$, $f=0.5$, $\omega=1.0$ and 1.5)

improved IHB method can efficiently and accurately obtain periodic solutions for nonlinear systems with time-delay state feedback. In addition, the IHB method can efficiently probe the unstable solution branches of nonlinear systems with time delays, whereas a numerical solver misses them entirely.

For the harmonically forced hard-spring Duffing oscillator with time-delay state feedback, the following can be concluded:

(1) When the time delay is considered, the peak of the primary resonance amplitude–frequency curve is shifted to the right. Furthermore, the whole amplitude–frequency curve of the 1/3 subharmonic resonance is shifted in the positive direction, and the frequency range of the 1/3 subharmonic resonance becomes much larger. This indicates that the nonlinearity of the system will become stronger after the time delay is considered.

(2) When the 1/3 subharmonic resonance occurs, the amplitude of the first-order harmonic will increase as the excitation frequency increases. Otherwise, the amplitude of the third-order harmonic decreases as the excitation frequency increases. The amplitude–frequency curve of the 1/3 subharmonic resonance is Fig. 8 shaped, and the stable and unstable segments intersect each other. Analysis showed that this is caused by the third-order harmonic vibration.

(3) The amplitude of the periodic solution can be effectively suppressed by increasing the feedback parameter, and the effect of the nonlinear spring is naturally weakened. There is a critical parameter for which the unstable periodic solution will disappear and hysteresis disappears.

(4) It can be intuitively seen from the time-delay effect matrix that the periodic solution changes periodically with the time delay, and the calculation results also verified this conclusion.

The conclusion of this paper can explain some nonlinear phenomena in actual mechanical system. In addition, the method proposed in this paper provides a reliable means for scholars to carry out quantitative analysis of nonlinear systems with time-delay feedback control, it can also be applied to high-dimensional strong nonlinear systems, thereby providing a foundation for the further study of time-delay nonlinear systems.

Acknowledgement This study was funded by the National Key R&D Program of China (Grant 2016YFB1200602), the National Natural Science Foundation of China (Grants 51805522, 11672306 and 51490673), the Strategic Priority Research Program of the Chinese Academy of Sciences (Grant XDB22020100) and the Informatization Plan of the Chinese Academy of Sciences (Grant XXH13506-204).

Declaration

Conflict of interest The authors declare that they have no known competing financial interests or personal relationships that could have appeared to influence the work reported in this paper. The authors declare the following financial interests/personal relationships which may be considered as potential competing interests.

References

1. Naik RD, Singru PM (2012) Stability and Hopf bifurcation of a Nonlinear oscillator with multiple time-delays. Chaos Solit Fract 45:1387–1396
2. Tian Z, Jiang J (2020) An active nonlinear controller emulating pendulum-type auto-parametric vibration absorber. J Vib Eng Technol 8:555–566
3. Hu H, Dowell EH, Virgin LN (1998) Resonances of a harmonically forced Duffing oscillator with time delay state feedback. Nonlinear Dyn 15(4):311–327
4. Cantis´an J, Coccolo M, Seoane JM, sanju´an MAF (2020) Delay-induced resonance in the time-delayed duffing oscillator. Int J Bifurcat Chaos 30(3): 2030007
5. Qiang YH, Qian YH, Guo XY (2019) Periodic solutions of delay nonlinear system by multi-frequency homotopy analysis method. J Low Freq Noise Vib Act Control 38(3–4):1439–1454
6. Bellizzi S, Chung KW, Sampaio R (2019) Response regimes of a linear oscillator with a nonlinear energy sink involving an active damper with delay. Nonlinear Dyn 97:1667–1684
7. Oishi S (2020) Numerical inclusion of exact periodic solutions for time delay Duffing equation. J Comput Appl Math 372:112620
8. Amer YA, El-Sayed AT, Kotb AA (2016) Nonlinear vibration and of the Duffing oscillator to parametric excitation with time delay feedback. Nonlinear Dyn 85:2497–2505
9. Siewe MS, Tchawoua C, Rajasekar S (2012) Parametric resonance in the Rayleigh-Duffing oscillator with time-delayed feedback. Commun Nonlinear Sci Numer Simul 17:4485–4493

10. Rusinek R, Weremczuk R, Kecik K, Warminski J (2014) Dynamics of a time delayed Duffing oscillator. Int J Non-Linear Mech 65:98–106
11. Wang YZ, Li FM (2015) Dynamical properties of Duffing–van der Pol oscillator subject to both external and parametric excitations with time delayed feedback control. J Vib Control 21(2):371–387
12. Mitra RK, Chatterjee S, Banik AK (2017) Limit cycle oscillation and multiple entrainment phenomena in a duffing oscillator under time-delayed displacement feedback. J Vib Control 23(17):2742–2756
13. Jin Y, Hu H (2008) Dynamics of a Duffng oscillator with two time delays in feedback control under narrow-band random excitation. J Comput Nonlinear Dyn 3(2):021205
14. Jin Y, Hu H (2007) Principal resonance of a Duffng oscillator with delayed state feedback under narrow-band random parametric excitation. Nonlinear Dyn 50(1):213–227
15. Jiang W, Shi H, Han X et al (2020) Double jump broadband energy harvesting in a helmholtz-duffing oscillator. J Vib Eng Technol 8:893–908
16. Lau SL, Cheung YK (1981) Amplitude incremental variational principle for nonlinear vibration of elastic systems. J Appl Mech 48:959–964
17. Mitra RK, Banik AK, Chatterjee S (2018) Response of a harmonically forced dry friction damped system under time-delayed state feedback. J Comput Nonlinear Dyn 13:031001
18. Shen YJ, Wen SF, Li XH, Yang SP, Xing HJ (2016) Dynamical analysis of fractional-order nonlinear oscillator by incremental harmonic balance method. Nonlinear Dyn 85(3):1457–1467
19. Wang Y, Zhang L, Zhou JX (2020) Incremental harmonic balance method for periodic forced oscillation of a dielectric elastomer balloon. Appl Math Mech (Engl Ed) 41(3):459–470
20. Cai M, Liu JK, Li J (2006) Incremental harmonic balance method for airfoil flutter with multiple strong nonlinearities. Appl Math Mech (Engl Ed) 27(7): 953–958
21. Liu YB, Xing YL, Law SS, Zhang YY (2017) Internal resonance vibration induced by nonlinearity of primary suspension system in high-speed vehicle system. Nonlinear Dyn 88(4):2947–2956
22. Wang S, Hua L, Yang C, Han X, Su Z (2019) Applications of incremental harmonic balance method combined with equivalent piecewise linearization on vibrations of nonlinear stiffness systems. J Sound Vib 441:111–125
23. Huang JL, Zhu WD (2017) A new incremental harmonic balance method with two time scales for quasi-periodic motions of an axially moving beam with internal resonance under single-tone external excitation. J Vib Acoust 139(2):021010
24. Li YL, Chen SY (2016) Periodic solution and bifurcation of a suspension vibration system by incremental harmonic balance and continuation method. Nonlinear Dyn 83(1–2):941–950
25. Lu CJ, Lin YM (2011) A modified incremental harmonic balance method for rotary periodic motions. Nonlinear Dyn 66(4):781–788
26. Ju R, Fan W, Zhu WD, Huang JL (2017) A modified two-time-scale incremental harmonic balance method for steady-state quasi-periodic responses of nonlinear systems. J Comput Nonlinear Dyn 12(5):051007
27. Cheung YK, Chen SH, Lau S (1990) Application of the incremental harmonic balance method to cubic non-linearity systems. J Sound Vib 140(2):273–286
28. Zhang XY (2013) Stability and delayed feedback control and experimental study of dynamical systems with time delay. Ph. D. dissertation, Tianjin University
29. Friedmann P, Hammond CE, Woo TH (1977) Efficient numerical treatment of periodic systems with application to stability problems. Int J Numer Meth Eng 11(7):1117–1136
30. Xu J, Chen YS (2004) Effects of time delayed velocity feedbacks on self-sustained oscillator with excitation. Appl Math Mech 25(5):499–512